Filter-Based Zeroth-Order Methods for Model-Free Voltage Control in Realistic Distribution Grids

Subir Majumder, *Member, IEEE,* Xin Chen, *Member, IEEE,* Le Xie, *Fellow, IEEE*

***Abstract*—Voltage regulation in power distribution systems encounters growing challenges due to the rapid proliferation of renewable distributed energy resources (DERs), characterized by their inherent variability, diverse ownership, and limited availability of reliable models for critical electricity infrastructure. The problem is further complicated by the scalability issue of coordinating numerous DERs. In this vein, this paper introduces a zeroth-order projected gradient method enhanced with high and low-pass filters for model-free optimal voltage control in three-phase unbalanced power distribution systems. As an integral component of the zeroth-order control approach, the proposed controller solely leverages a finite set of voltage measurements to derive control actions, presenting a plug-and-play solution. In this regard, extensive numerical experiments conducted on an Austin Grid test feeder, utilizing realistic datasets, demonstrate the model-free controller's seamless integration with conventional, slow-acting voltage regulation devices. The resilience, robustness, and feasibility of deploying the proposed controller are also studied. Furthermore, the algorithm's performance is evaluated under a simulated Denial of Service (DOS) attack.**

***Index Terms*—Model-free control, projected gradient descent, voltage control, zeroth-order methods.**

I. Introduction

As more and more distributed renewable energy resources (DER) are being integrated into the distribution systems, it is crucial to develop scalable algorithms that facilitate voltage control in multi-device, multi-vendor, multi-technology, and multi-owner systems and support plug-and-play operation with reduced communication. Distributed voltage control algorithms are one such approach, however, among the related algorithms reported in the literature, most iterative algorithms are gradient-based [1]. These algorithms offer several advantages such as plug-and-play capability, privacy preservation, self-organization, and reduced communication. However, these algorithms heavily rely on accurate power system models, even though recent feedback-based algorithms [2]–[5] can partially circumvent this requirement. On the contrary, local control approaches [6] do not require frequent communication, but their reliance on droop-based strategies compromises optimality.

The widespread deployment of smart meters and information and communication technologies (ICTs) paves the way for data-driven control techniques. Reinforcement learning (RL) is one such data-driven/model-free method that has gained significant attention in recent years (see [7] for a thorough literature review). However, RL faces several fundamental limitations, including safety requirements, scalability issues, training efficiency, and limited theoretical guarantees [8]. On the other hand, zeroth-order (ZO) methods (also known as extremum seeking control) mitigate these limitations and have gained considerable attention for solving optimal model-free control problems [9], [10]. ZO methods learn the gradient of an objective function only based on function evaluations or system measurements [11] and hence do not require system model information, thus solving challenges of distributed algorithms as well as RL algorithms. Moreover, ZO control methods can self-adapt to dynamic environments, such as fluctuating renewable generation and changing power network topology, and operate in a plug-and-play fashion, with theoretical performance guarantees on stability and robustness [12]. ZO control has been applied in various domains, such as distribution network voltage control [13], [14], maximum power point tracking in solar systems [15], and hardware-in-the-loop systems [16].

Based on the number of function evaluations made during each iteration, ZO methods can be classified into two categories: single-point and multi-point [17]. Single-point ZO (SZO) methods require only a single function value query per iteration. This characteristic renders them particularly suitable for online optimization and dynamic control problems. However, SZO methods generally suffer from large estimation variance and slow convergence, which pose substantial obstacles to their practical application. To address this issue, the recent work [18] borrows the idea of high-pass and low-pass filters and develops a novel SZO method called HLF-SZO (High/Low-pass Filter SZO) by integrating these filters. The HLF-SZO method exhibits much smaller variances and achieves the fastest convergence in the category of SZO methods to date, with both theoretical guarantees and empirical demonstration. This facilitates the application of SZO methods to real-world system control problems. Nevertheless, the HLF-SZO method in [18] focuses on unconstrained optimization problems, and further research is required to bridge the gap between theoretical work and practical applications.

Contributions. In this paper, we adapt the HLF-SZO method developed in [18] to the optimal voltage control (OVC) problem in realistic distribution systems for addressing the critical issue of unknown system models. The main contributions of this paper are summarized as follows:

(1) The HLF-SZO method proposed in [18] only considers a simple unconstrained optimization problem setting. Built upon this, our paper develops a novel filter-based SZO algorithm, called HLF-SZO-PGD, by integrating HLF-SZO with the projected gradient descent (PGD) method. This proposed HLF-SZO-PGD algorithm can solve *constrained* optimization problems in a model-free manner.

(2) This paper adapts the proposed HLF-SZO-PGD algorithm to the real-time model-free voltage control in three-phase unbalanced distribution systems. Our voltage control algorithm does not require any system model information,

S. Majumder, X. Chen, and L. Xie are with the Department of Electrical Engineering and Computer Sciences, Texas A&M University, USA. (Corresponding author e-mail: subir.majumder@tamu.edu).

This work is supported in part by the Texas A&M Engineering Smart Grid Center and Texas A&M Energy Institute.

and can self-adapt to the changing system conditions and operate in a plug-and-play fashion.

(3) To assess the practical performance of our algorithm, we build a high-fidelity testbed simulator based on OpenDSS [19], and employ a realistic three-phase unbalanced 127-node Austin distribution feeder with real load and generation data as the test system. The code and data will be made open-source[1]. Moreover, extensive numerical experiments are conducted to demonstrate the convergence and robustness of our algorithm, including time-varying system environment, noisy measurement, and the presence of cyber-attacks such as Denial of Service (DoS) attacks.

The remainder of this paper is structured as follows. Section II formulates the voltage control problem and develops the SZO-based voltage control algorithms. Section III describes the testbed and the configuration of the Austin distribution feeder. Section IV presents the numerical experiment results, and Section V concludes this work.

Notation. Unbolded lower-case letters are used for scalars, and bolded lower-case letters are for vectors. $||(\cdot)||$ denotes the L_2 norm of a vector. The projection of a point $x \in \mathbb{R}$ onto the set χ is defined as $\mathcal{P}_\chi(x) := \arg\inf_{y\in\chi}||y - x||$.

II. Problem Formulation and Algorithms

In this section, we introduce the OVC problem formulation and present the zeroth-order control algorithms with high-pass and low-pass filters.

A. Optimal Voltage Control in Power Distribution System

Consider a three-phase unbalanced power distribution network with the set of monitored bus $\mathcal{M}$ and the set of controllable bus $\mathcal{C}$. Each bus $j \in \mathcal{M}$ has real-time voltage measurement $v_{j,\phi}^{meas}$ at each available phase $\phi \in \{A, B, C\}$. The reactive power injection q_i^ϕ of phase ϕ at each controllable bus $i \in \mathcal{C}$ is the decision variable and can be controlled separately across phases for voltage regulation. Let $\boldsymbol{q}_i := (q_i^\phi)_{\forall\phi}$ be the vector that collects the per-phase reactive power injections at bus i. The OVC problem is formulated as model (1):

$$\min_{\boldsymbol{q}} h(\boldsymbol{q}) := c \sum_{\forall j\in\mathcal{M}} \sum_{\forall\phi} (v_{j,\phi}(\boldsymbol{q}) - v_j^{sp})^2 + \sum_{\forall i\in\mathcal{C}} \sum_{\forall\phi} d_i (q_i^\phi)^2, \tag{1a}$$

$$\text{s.t. } \boldsymbol{q}_i \in \mathcal{Q}_i, \quad i \in \mathcal{C}. \tag{1b}$$

Here, c and d_i are the cost parameters associated with voltage deviation and for providing reactive power. v_j^{sp} is the specified desired voltage level of bus j, around which the voltage should be maintained. The objective function (1a) encompasses two components: the deviation of the observed voltage magnitudes at the monitored buses $j \in \mathcal{M}$, and the opportunity cost associated with participating in voltage regulation at the controllable buses $i \in \mathcal{C}$ (see [6] for more details). The decision variable $\boldsymbol{q}_i$ at each bus $i \in \mathcal{C}$ is constrained by the feasibility set $\mathcal{Q}_i$ (could be decoupled across phases), which represents the power capacity of individual devices and is defined by (2)-(4):

$$\boldsymbol{q} := (\boldsymbol{q}_i)_{\forall i\in\mathcal{C}}, \quad \boldsymbol{\mathcal{Q}} := \prod_{\forall i\in\mathcal{C}} \mathcal{Q}_i. \tag{2}$$

[1]Not included to preserve anonymity per the journal's policy.

We consider two types of controllable devices whose reactive power injections can be adjusted for voltage control: (i) devices that only inject reactive power, and (ii) devices that inject both real and reactive power. The former type includes devices such as Static Var Compensators (SVCs) and Distribution Static Synchronous Compensators (D-STATCOMs), which can adjust reactive power injection by controlling the firing angle, and their capabilities are bounded by the device per phase power rating $[\underline{q}_i^\phi, \bar{q}_i^\phi]$. Hence, the associated feasibility set is defined as:

$$\mathcal{Q}_i := \{\boldsymbol{q}_i | \, \underline{q}_i^\phi \le q_i^\phi \le \bar{q}_i^\phi\}. \tag{3}$$

Distributed generators (DGs) belong to the other category, where they are capable of injecting both real and reactive power into the grid. Their reactive power injection is further constrained by the per phase apparent power rating $\bar{s}_i^\phi$ and *pre-determined* active power injection $p_i^{o,\phi}$. Storages also fall under this category, where other algorithms control active power injections. While both active and reactive power could contribute to voltage control [5], [6], [8], this work is limited to reactive power only. The associated feasibility set is given by:

$$\mathcal{Q}_i := \{\boldsymbol{q}_i | \, \underline{q}_i^\phi \le q_i^\phi \le \bar{q}_i^\phi, (p_i^{o,\phi})^2 + (q_i^\phi)^2 \le (\bar{s}_i^\phi)^2\}. \tag{4}$$

The functional form $v_{j,\phi}(\boldsymbol{q})$ in (1) implies that reactive power injections across all the phases throughout the network affect system-wide voltages. Moreover, the function $\boldsymbol{v}(\boldsymbol{q}) := (v_{j,\phi}(\boldsymbol{q}))_{\forall j\in\mathcal{M},\forall\phi}$ captures the entire power distribution system model, non-convex power flow equations, and uncontrollable loads and renewable generations [20]. However, in practice, accurate distribution system models are often unavailable and subject to change due to deliberate network reconfiguration and unforeseen disturbances. Therefore, in this paper, we consider the problem setting where the function (or system model) $\boldsymbol{v}(\boldsymbol{q})$ is *unknown*. Nevertheless, the real-time voltage measurement $v_{j,\phi}^{meas}$ is available for the monitored buses $j \in \mathcal{M}$, which can be leveraged as system feedback to circumvent the distribution system model for voltage control.

To solve the OVC problem (1), we first introduce the *Projected Gradient Descent (PGD)* algorithm [20]:

$$\boldsymbol{q}_i(t+1) = \mathcal{P}_{\mathcal{Q}_i}\Big[\boldsymbol{q}_i(t) - k\frac{\partial h(\boldsymbol{q})}{\partial \boldsymbol{q}_i}\Big], \quad i \in \mathcal{C}, \tag{5}$$

where k is the stepsize and each component in $\frac{\partial h(\boldsymbol{q})}{\partial \boldsymbol{q}_i}$ is

$$\frac{\partial h(\boldsymbol{q})}{\partial q_i^\phi} := 2c \sum_{\forall j\in\mathcal{M}} \sum_{\forall\phi'} (v_{j,\phi'}(\boldsymbol{q}) - v_j^{sp}) \frac{\partial v_{j,\phi'}(\boldsymbol{q})}{\partial q_i^\phi} + 2d_i q_i^\phi. \tag{6}$$

As a part of the PGD, the controller computes the gradient $\frac{\partial h(\boldsymbol{q})}{\partial q_i^\phi}$ at each discrete time step t to determine the control action at the next step $t+1$. By using the projection $\mathcal{P}_{\mathcal{Q}_i}(\cdot)$, the PGD algorithm (5) ensures that $\boldsymbol{q}_i$ always stays within $\mathcal{Q}_i$ at all iterations. Under regular convexity conditions on the OVC problem (1), the PGD algorithm (5) can iteratively converge to an optimal solution of (1) [21]. However, the PGD algorithm (5) is not implementable, as $v_{j,\phi'}(\boldsymbol{q})$ and $\frac{\partial v_{j,\phi'}(\boldsymbol{q})}{\partial q_i^\phi}$ in (6) require the unknown system model $\boldsymbol{v}(\boldsymbol{q})$. Furthermore, the underlying system model $\boldsymbol{v}(\boldsymbol{q})$ is time-varying due to the variations in loads, distributed generations, as well as system disturbances. To address the issue of the absence of the model,

in the following, we develop the ZO methods based on the PGD algorithm for voltage control. It is notable that q_i^ϕ is readily available to the controllers and need not be estimated, and we will utilize this feature in the algorithm development.

Remark 1. *While the model* (1) *adopts a quadratic function to regulate voltages at monitored buses, alternative convex functions can also be used. Moreover, beyond the current framework, constraints can be applied to other power distribution system parameters, like branch flows.*

B. Extremum Seeking Control Based Voltage Control

Extremum-seeking control is regarded as the continuous-time version of ZO methods, which estimates the gradients based on only function evaluations or system outputs. Below, we first present the preliminaries of extremum-seeking control and then develop ZO algorithms for voltage control. In this paper, we focus on the *discrete-time* version of ZO methods.

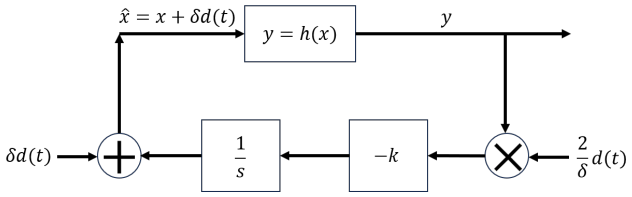

Fig. 1. A classic extremum seeking control algorithm.

Consider solving the optimization problem $\min_x h(x)$ with an unknown static mapping function $y = h(x)$. The simplest solution of extremum seeking control with the necessary components is illustrated as the block-diagram in Fig. 1. It is expected to find the optimal operating point of the plant with the unknown static map (operating conditions do not change over time) over time t. In this regard, a small dither or probing signal $\delta d(t)$ is added to the state x to estimate the gradient $h'(x)$ using only output feedback. The closed-loop dynamics of the extremum-seeking system is formulated as:

$$\dot{x} = -k \cdot \frac{2}{\delta} h\left(x + \delta d(t)\right) d(t). \tag{7}$$

Here, $d(t)$ is the probing signal with an amplitude of $\delta > 0$. $y = h(x)$ represents the plant, while $\frac{1}{s}$ and $-k$ are the integrator and gain, respectively. Typically, the probing signal is periodic with a period of T and satisfies (8):

$$\int_0^T d(t)\, dt = 0;\ \frac{1}{T}\int_0^T d^2(t)\, dt > 0;\ \max_{t\in[0,T]} |d(t)| = \delta. \tag{8}$$

Commonly used probing signals include sinusoidal, triangular, and square waves [22]. See [9] for more explanations. In this paper, we consider sinusoidal probing signals $d(t) := \delta \sin(\omega t)$ with the frequency parameter ω.

Using the Taylor expansion and the averaging theory, the average system dynamics of (7) is derived as:

$$\begin{aligned}\dot{x} &= -\frac{k}{T}\int_0^T \frac{2}{\delta} h\left(x + \delta \sin(\omega t)\right) \sin(\omega t) dt \\ &= -\frac{k}{T}\int_0^T 2\sin^2(\omega t) h'(x) + \mathcal{O}(\delta) dt = -k h'(x) + \mathcal{O}(\delta).\end{aligned} \tag{9}$$

Equation (9) implies that the average dynamics of the extremum seeking system (7) is indeed a gradient descent dynamics together with a small perturbation $\mathcal{O}(\delta)$. See [10] for detailed analysis on the extremum-seeking system.

The above problem setting and control methods can be extended to multi-port (multi-input-multi-output) systems, where different frequency parameters $\boldsymbol{\omega} := (\omega_i)_{i\in\mathcal{C}}$ need to be used for different control input variables. Moreover, the frequency parameters need to satisfy $\omega_i \neq \omega_j$, $\omega_i + \omega_j \neq \omega_k$ for any $i, j, k \in \mathcal{C}$ [11]. It's key to recognize that *the distribution network functions as a multi-port system, allowing for straightforward implementation of ZO control. This also necessitates unique ω_i^ϕ values for each phase.*

Algorithm 1 SZO-PGD-Based Model-Free Optimal Voltage Control (OVC) Algorithm.

At each time step t, do the following steps:

- **Each monitored node** $j \in \mathcal{M}$ measures local voltage magnitude $(v_{j,\phi}^{meas}(t))_{\forall\phi}$ and sends it to all controllable nodes.
- **Each controllable node** $i \in \mathcal{C}$ calculates:

$$h_t^i = c \sum_{j\in\mathcal{M}} \sum_{\phi} (v_{j,\phi}^{meas}(t) - v_j^{sp})^2, \tag{10a}$$

$$\boldsymbol{q}_i(t+1) = \mathcal{P}_{\mathcal{Q}_i}\Big[\boldsymbol{q}_i(t) - k\big(\frac{2}{\delta} h_t^i \sin(\boldsymbol{\omega}_i t) + 2 d_i \boldsymbol{q}_i(t)\big)\Big], \tag{10b}$$

then deploy the reactive power injection $\hat{\boldsymbol{q}}_i(t+1)$:

$$\hat{\boldsymbol{q}}_i(t+1) = \boldsymbol{q}_i(t+1) + \delta \sin(\boldsymbol{\omega}_i(t+1)), \tag{11}$$

where $\boldsymbol{\omega}_i := (\omega_i^\phi)_{\forall\phi}$ and $\sin(\boldsymbol{\omega}_i t) := (\sin(\omega_i^\phi t))_{\forall\phi}$.

While the analysis in (9) is provided for a continuous time system, the dynamics of the extremum-seeking system for a discrete-time system can be suitably obtained. Consequently, the PGD algorithm (5) can be modified as an *SZO-PGD* method for voltage control, which is outlined in Algorithm 1. Compared with the PGD algorithm (5), the SZO-PGD method (10) estimates the gradient of the first part of the objective function (1a) using only function evaluations. Ideally, without consideration of measurement noises, the voltage measurement $v_{j,\phi}^{meas}(t) = v_{j,\phi}(\hat{\boldsymbol{q}}(t))$ represents the real-time system feedback to the reactive power injections[2]. In this way, the SZO-PGD-based optimal voltage control algorithm (Algorithm 1) does not require the distribution system model information (model-free) but only needs the voltage measurement to perform. Under regular conditions, one can show that Algorithm 1 can steer the reactive power decision $\boldsymbol{q}$ *towards*[3] an optimal solution of the OVC problem (1); see [9] for more explanations. Algorithm 1 is referred to as an SZO method as it queries the voltage function (or measurement) only once at each iteration.

C. Zeroth-Order Control with High-Pass and Low-Pass Filters

The above SZO-PGD method is a model-free approach that can circumvent the system model information. However, it suffers from large oscillations and slow convergence, which are the fundamental limitations of SZO methods and seriously hinder practical applications. To address these challenges, we

[2]We study the impact of noisy measurement on the algorithm performance in Section IV-B.

[3]Algorithm 1 drives the reactive power decision $\boldsymbol{q}$ to a small $\mathcal{O}(\delta)$-neighbor of an optimal solution of the OVC problem (1) instead of a fixed optimal point, as a small probing signal $\delta\sin(\boldsymbol{\omega}_i t)$ is continuously added to $\boldsymbol{q}_i$ in (11).

develop a novel filter-based SZO algorithm, HLF-SZO-PGD, by integrating the HLF-SZO method introduced in [18] to Algorithm 1 for voltage control. The HLF-SZO-PGD-based model-free OVC method is presented as Algorithm 2.

Algorithm 2 HLF-SZO-PGD-Based Model-Free Optimal Voltage Control (OVC) Algorithm.

At each time step t, do the following steps:

- **Each monitored node** $j \in \mathcal{M}$ measures local voltage magnitude $(v_{j,\phi}^{meas}(t))_{\forall \phi}$ and sends it to all controllable nodes.
- **Each controllable node** $i \in \mathcal{C}$ calculates:

$$\text{Equation(10a)}, \ \gamma_t^i = h_t^i - h_{t-1}^i, \tag{12a}$$

$$\boldsymbol{q}_i(t+1) = \mathcal{P}_{\mathcal{Q}_i}\Big[\boldsymbol{q}_i(t) - k\big(\frac{2}{\delta}\gamma_t^i \sin(\boldsymbol{\omega}_i t) + 2d_i \boldsymbol{q}_i(t)\big) + \alpha\big(\boldsymbol{q}_i(t) - \boldsymbol{q}_i(t-1)\big)\Big], \tag{12b}$$

then deploy the reactive power injection $\hat{\boldsymbol{q}}_i(t+1)$ (11).

Compared with Algorithm 1, Algorithm 2 replaces the reactive power update rule (10b) with (12). Equation (12a) results from the integration of a high-pass filter, where γ_t^i is the residual difference between the function evaluation h_t^i at time t and the function evaluation h_{t-1}^i one time step earlier. Here, γ_t^i can be viewed as a refined value of the function evaluation h_t^i after passing through a high-pass filter, which can significantly mitigate the transient oscillations. In (12b), an additional term $\alpha\big(\boldsymbol{q}_i(t) - \boldsymbol{q}_i(t-1)\big)$ is added, where $\alpha \in [0, 1]$ is an tunable parameter. This additional term results from the integration of a low-pass filter and can be interpreted as the "momentum" method [23], which can further accelerate the convergence [18]. The HLF-SZO-PGD method (12) does not need the system model (model-free) to perform as well, and it is an SZO method as the values of h_{t-1}^i and $\boldsymbol{q}_i(t-1)$ can be directly recycled from the memory of the last iteration. In Algorithm 2, each controller receives all the voltage measurements and calculates h_t^i according to (10a). In (12b), the term $\frac{2}{\delta}\gamma_t^i \sin(\boldsymbol{\omega}_i t)$ is the ZO gradient estimator for the quadratic voltage deviation penalty.

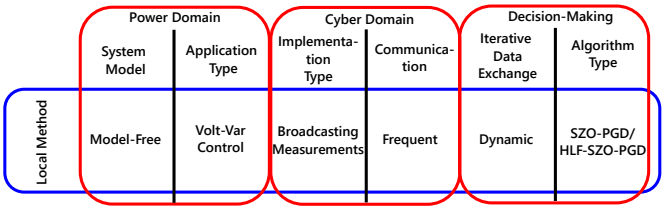

Fig. 2. Taxonomy of the **SZO-PGD/HLF-SZO-PGD** algorithm.

Based on the scope and control implementation, a taxonomy of the above SZO control algorithms is presented in Fig. 2, which summarizes the key features of these algorithms [6]. In particular, the proposed HLF-SZO-PGD algorithm is fully model-free, and it does not need the parameters or topologies of the power networks, which estimates the gradients solely based on real-time measurements. It also enables plug-and-play operation and does not require a control center for coordinating a large amount of distributed energy devices. Essentially, the proposed HLF-SZO-PGD algorithm mimics the PGD algorithm for solving constrained optimization problem, while estimating the unknown gradients using SZO methods. Hence, in theory, the convergence of HLF-SZO-PGD should be no superior to that of the PGD algorithm. References [17], [18] provide comparisons of convergence rates across various types of ZO methods for solving unconstrained optimization problems. However, there is limited work [24] on convergence analysis of ZO methods for solving constrained optimization problems. We demonstrate the convergence properties of HLF-SZO-PGD through extensive numerical experiments.

Remark 2. In contrast to the HLF-SZO method in [18], the HLF-SZO-PGD method (i.e., Algorithm 2) proposed in this paper represents a substantial extension, enabling it to effectively solve constrained optimization problems. Furthermore, compared with the existing work [8] on model-free ZO voltage control, this paper exhibits three major advantages: 1) In [8], only a low-pass filter is used, while our method integrates both high-pass and low-pass filters, leading to superior performance, as demonstrated by our simulations; 2) The work in [8] is formulated based on continuous-time dynamics, while our method is an iterative algorithm and thus is more suitable for practical implementation; and 3) This paper expands upon the work [8] by extending the application of voltage control to *three-phase unbalanced* distribution systems with much more realistic settings and comprehensive testings. □

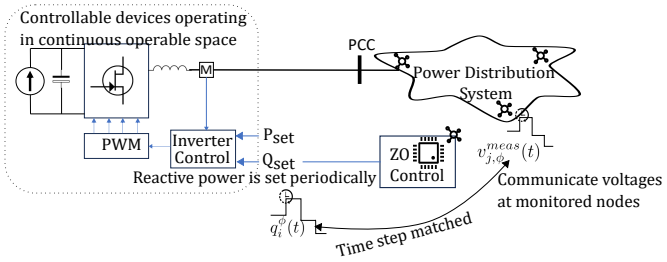

Fig. 3. Discrete time control action.

Practical Implementation. The implementation of the ZO algorithms above has been illustrated in Fig. 3. The controllable device consists of an energy source, power electronic switches, measurements to determine references for the control of these switches, and a pulse width modulation (PWM) generator for driving the converters. The controllable devices are connected to the rest of the grid through the point of common coupling (PCC). The inverter control part also takes in both active and reactive power setpoints, P_{set} and Q_{set}, respectively. In our case, Q_{set} is driven by the ZO controller. Given that Algorithm 2 operates in discrete time steps, it can be expected that between any two time intervals, the reactive power setpoint Q_{set}, namely $\hat{\boldsymbol{q}}_i(t)$, remains constant, which is also highlighted in the staircase function in the diagram. As shown in the diagram and Algorithm 2, the controller solely relies on the unidirectional broadcasted voltage magnitudes across the system. Communication burdens are significantly reduced, given the voltage measurements are broadcasted. Voltages are measured and communicated once within a time-step, which makes the voltage magnitude appear to be a staircase function as well. Given that the step size of the algorithm is known, in an IP-based communication, the controllers can match the time steps across received voltage measurements to calculate reactive power set-points.

Moreover, the controllers require various inputs at the time

of integration. These inputs include all model parameters such as c and d, specified voltages v_j^{sp}, and algorithm-specific parameters like δ, k, and α. Additionally, there's a requirement to negotiate values for ω_i^{ϕ} during the connection process.

III. Configuration of Austin Grid

We have demonstrated and compared the performance of the proposed algorithms on two distinct systems: 1) the IEEE 13-bus system and 2) a realistic test feeder emulating an actual system situated in Austin, Texas, as detailed in [25]. The test feeder represents a 3-phase unbalanced distribution network encompassing 127 nodes, each varying in the number of phases per node. The feeder's topological structure is depicted in Fig. 4, with specific node names highlighted that are used in controller performance analysis. We have renamed these nodes to improve the readability of the figures. Our synthesized feeder is further enhanced to incorporate a substation equipped with a 12.47 kV/7.20 kV, 7 MVA transformer with on-load tap-changer (OLTCs) alongside other distribution nodes operating at 480 V and 240 V. An additional static voltage regulator (SVR) is integrated, as illustrated in Fig. 4, to maintain voltage levels within defined thresholds with large penetration of PV resources.

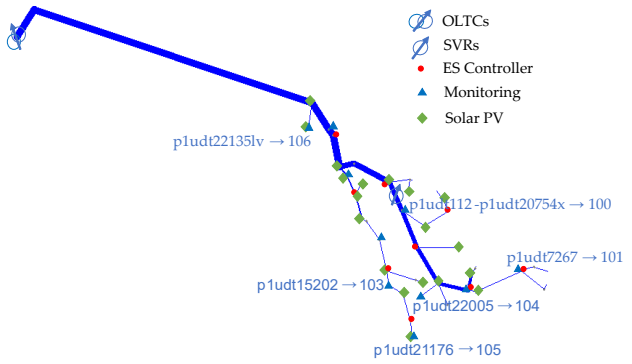

Fig. 4. The test feeder from the synthetic Austin Grid.

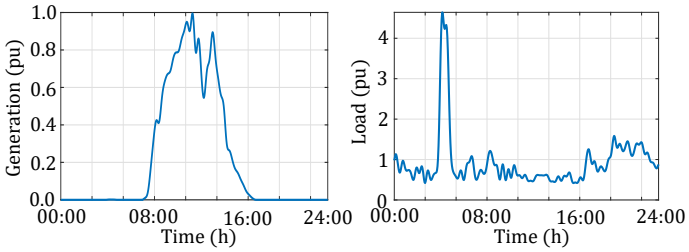

Fig. 5. The solar and load profiles in a typical day.

The nodes interfacing with solar PV installations, as well as the controllers, are depicted in Fig. 4. Given that the proposed ZO controllers respond to the measured voltage across the system, the monitored nodes are also shown. These nodes broadcast the voltage information to all controllers, and notably, a new controller is just required to derive the control signal from these broadcasts alone. These controllers are also not required to know the operating conditions of OLTCs and SVRs, as demonstrated in Algorithms 1 and 2. Furthermore, the load and PV-generation profiles utilized for testing are sourced from real data provided by Pecan Street [26], representative of the Austin, Texas region. As shown in Fig. 5, the inclusion of sudden load and generation profile spikes in the time-varying scenarios could assist in the assessment of the controller's robustness. In addition, *OpenDSS* [19] is used as the system simulator capturing the full nonlinear non-convex power flow equations, with pre-calculated setpoints for the OLTCs and SVRs already deployed.

As a part of quasi-static simulation and to capture the fast variation in the load and generation, we assume a 2-second timescale for ZO controller operations. In light of the broadcasting requirements from monitoring nodes, the likelihood of encountering data packet corruption, missing measurements, noisy voltage data, and cyber-attacks is a major concern. For the cyber anomalies, we focus on denial of service (DOS) attacks. Implementation details of various data- and cyber-anomalies are given below and will be used in the following section as a part of case studies:

Noisy Measurements: ZO methods show robustness to small additive noises while maintaining similar convergence results [12]. However, numerical simulations are needed for large measurement noises and testing in a realistic environment when the assumptions used for the ZO controller do not hold. Specifically, we have introduced a Gaussian noise of zero mean and standard deviation of 1%, 5%, and 7% to test the robustness of the controller.

Missing/Corrupted Measurements/DoS: Communication channel could be non-ideal, and the broadcasted measurement may arrive prematurely, appear corrupted, or be missing within the controller's time step. If the measurements appear earlier, they could be stored within a buffer inside the controller. In the event of missing measurements, the ZO controller utilizes past measurements or a pseudo measurement of 1 *pu* for set-point calculation.

Notably, an anomaly detection layer could be positioned between the controller and measurement reception unit aimed at identifying potential anomalies and taking corrective actions to enhance controller performance cyber attacks [6].

IV. Implementation and Results

In the context of a multi-port system representing a distribution network, we have strategically selected probing signal frequencies based on prime numbers. While the exact methodology to calculate these probing signals is not demonstrated for simplicity, it could be easily accessed from the shared repository. We define this set of frequencies to be ω (with units rad/iterations or rad/s). In the experiments to analyze the convergence of the algorithms, we considered a fixed PV injection of 0 *pu* and a system-wide load of 3 *pu* to understand the convergence characteristics of the controllers. The simulation results are shown in Fig. 6. Notably, both controllers ensured that the steady-state voltage profile remained within acceptable bounds (see Figs. 6(a.2-3) and 6(b.2-3)).

Given the voltage measurements with algorithm *SZO-PGD* shown in Figs. 6(a.2) and 6(b.2), it can be seen that the introduction of filters into the *SZO-HLF-PGD* algorithm notably attenuated high-frequency perturbations in voltage measurements, as demonstrated in Figs. 6(a.3) and 6(b.3). For the *SZO-PGD* algorithm, there has been a presence of the larger oscillation in the computed gradient, which limits the choice of stepsize. Contrarily, in the filter-based technique, one could

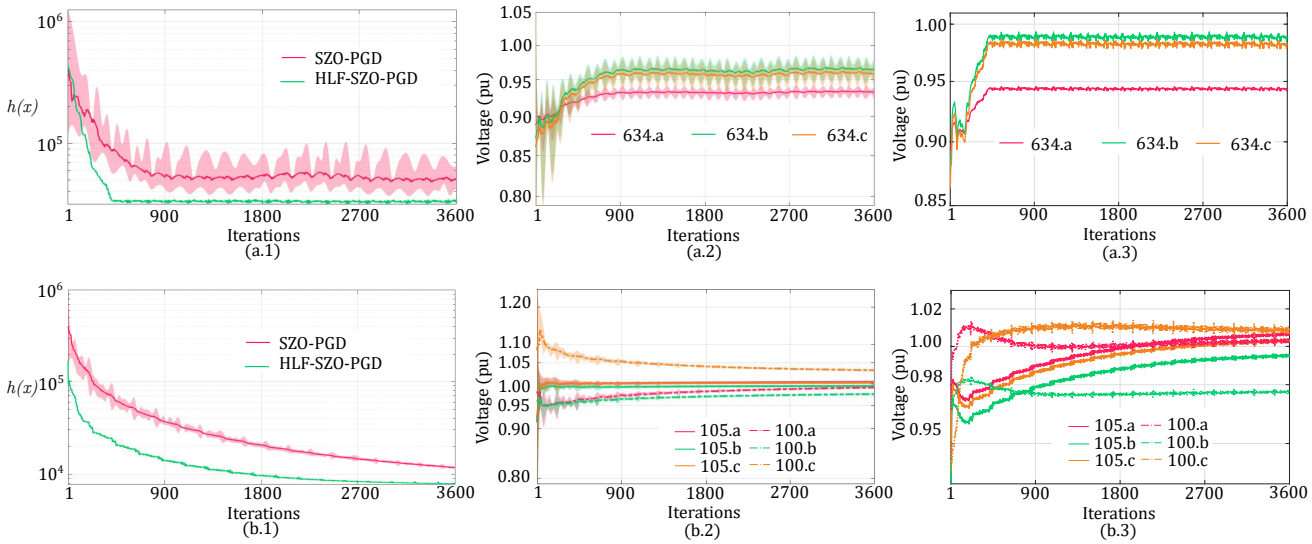

Fig. 6. Algorithm performance under constant load for both IEEE 13-node (a.1-a.3) and synthetic Austin grid (b.1-b.3).

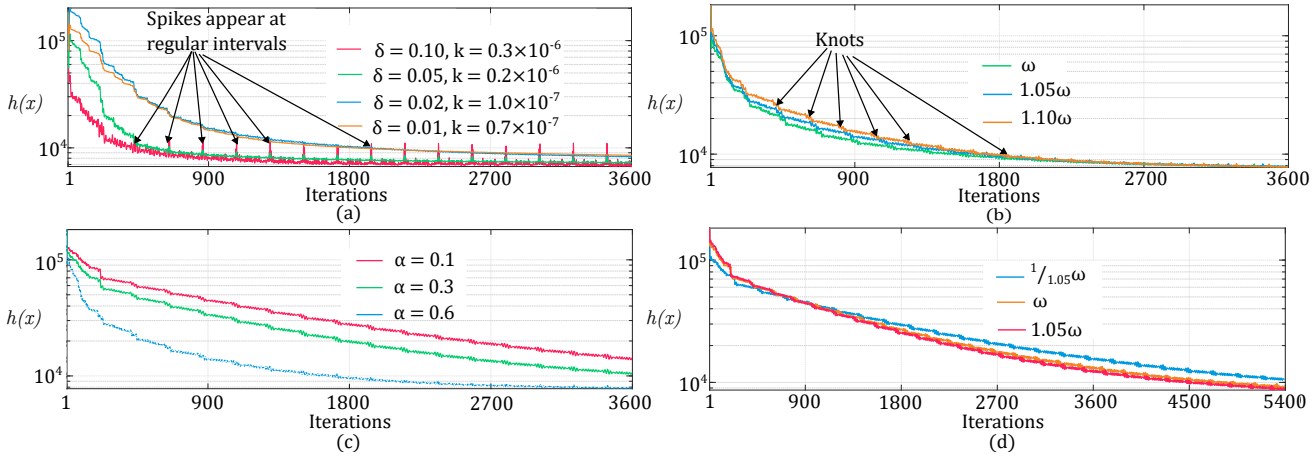

Fig. 7. Parametric analysis of *SZO-HLF-PGD* algorithm considering synthetic Austin grid with constant load demand.

choose a higher step size, which can lead to rapid convergence of the algorithm, as demonstrated in Figs. 6(a.1) and 6(b.1). For example, for the IEEE 13-node case, with filters, $\delta = 0.1$ and ω, one could increase step-size from 0.42×10^{-6} to 0.90×10^{-6} with $\alpha = 0.9$ to reduce the convergence time from 900 iterations to $\sim$ 450 iterations. For the Austin grid case, with filters, $\delta = 0.03$ and ω, the step-size could be increased from 0.3×10^{-7} to 10^{-7} with $\alpha = 0.6$ to reduce the convergence time to 1800 iterations (for voltages).

Given the iterative nature of the algorithms, there can be multiple of these hyperparameters (δ, k, α, and ω) that dictate the convergence. In the next subsection, we will analyze the same while limiting our focus to the Austin grid case.

A. Parametric Analysis

1) Impact of Probing signal Amplitude (δ) and step size (k) on Convergence: The idea of ZO controller revolves around the timescale separation property among the fast dynamics of control variables, the dynamics of the probing signal, and the dynamics of controller convergence [27]. From (9), if δ is small, the average dynamics estimates the gradient accurately. However, using a larger δ is expected to compute the gradient better. Consequently, comparing all four cases in Fig. 7(a), it can be seen that higher δ allows us to use higher k for faster convergence. We observe that increasing δ would also introduce significant perturbation in the systemwide voltage (with larger δ and k, we observe spikes/knots appear in the objective function as shown in Fig. 6(b.2)). This is also reflected in the objective function shown in Fig. 7(a). Therefore, for practical implementation, δ and k can not be too high. We have performed these experiments with $\alpha = 0.6$ and ω.

2) Impact of Filters: High pass filters are embedded into the algorithm through (12a), and are not therefore controllable. The strength of the low-pass filter can be dictated by the choice of α, with $\alpha = 0$ leading to a vanishing low-pass filter. As shown in Fig. 7(c), the algorithm converges faster with increasing $\alpha (> 0)$, similar to [18]. However, increasing α may harm algorithm performance by interfering with slow time-

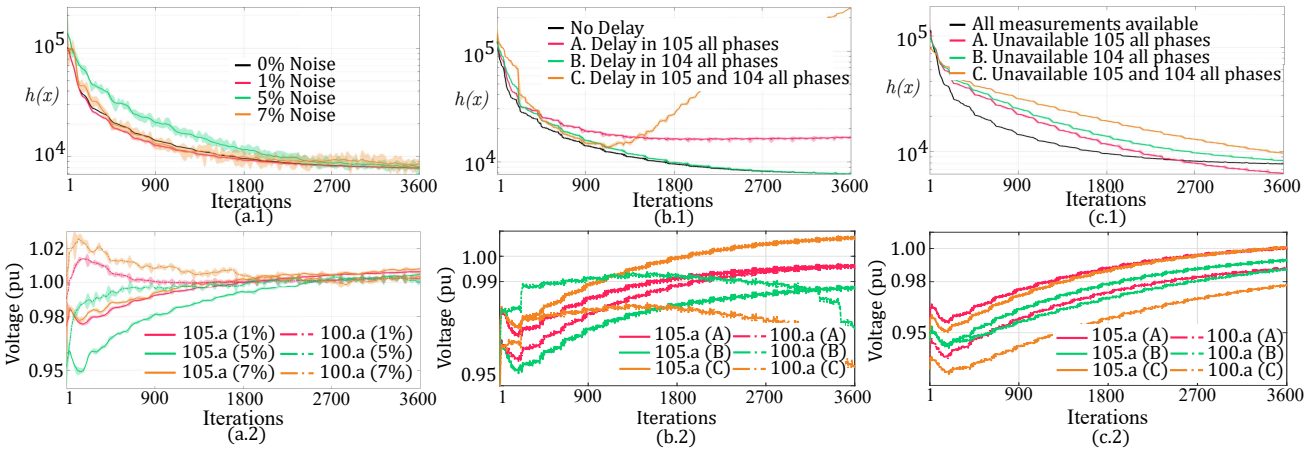

Fig. 8. Robustness of *HLF-SZO-PGD* algorithm with constant load under different scenarios: (a) noise, (b) delay in measurements, (c) missing measurements. The voltages shown in this figure correspond to Phase A only.

scale gradient-learning dynamics. We have performed these experiments with $\delta = 0.03$, $k = 1.0 \times 10^{-7}$ and ω.

3) Impact of Probing Signal Frequency (ω) on Convergence: Typically, larger ω would lead to better time-scale separation property [27], leading to faster convergence. However, its impact is limited by the choice of low-pass filters. In this regard, we have tested the algorithm against $\alpha = 0.6$ with three sets of probing signals, ω, 1.05ω, and 1.10ω and the results are provided in Fig. 7(b). We have also performed experiments with $\frac{1}{1.05}\omega$, ω, and 1.05ω with $\alpha = 0.1$. In both cases, we have chosen $\delta = 0.03$, and $k = 1 \times 10^{-7}$ (see Fig. 7(d)).

With the lower value of α, the convergence of the algorithm gets enhanced with increasing probing signal frequency; however, with higher α, convergence deteriorates with increasing probing signal frequency. Selected probing signal frequencies do not exert a discernible influence on the optimal solutions. Pushing probing signal frequencies beyond a certain threshold may induce divergence (not presented here for brevity).

B. Algorithmic Robustness

Here, we systematically assess the performance of the *SZO-HLF-PGD* algorithm under the distinct test conditions within the synthetic Austin grid while considering consistent probing signals and hyper-parameter settings ($\delta = 0.03$, ω, $\alpha = 0.6$, $k = 1 \times 10^{-7}$). Based on the discussion in Section III, we tested the algorithm convergence considering (a) noisy measurements, (b) delayed measurements, and (c) unavailable data. In scenarios where data are unavailable, the controller is assumed to rely on a default measurement value of 1 *pu*. The simulation results are illustrated in Fig. 8. We have visualized only the phase-a voltages for brevity.

For the noisy measurement test case, we introduce measurement noise levels of 1%, 5%, and 7% across all available measurements. Trajectories of objective functions (see Fig. 8(a.1)) and the voltages in the presence of varying measurement noise (see Fig. 8(a.2)) reveal that increasing measurement noise levels appear to exert no discernible impact on convergence (all three cases converge within 1800 iterations as with no noise scenario), although the oscillations in the objective function tend to increase with increasing noise level. It can be expected that the controller may diverge with large measurement noises.

In the delayed measurements scenario, we introduce a fixed 3-sample delay in voltage measurements across all phases from a designated node. We examine three distinct cases: (i) measurement delay from node '105,' (ii) measurement delay from node '104,' and (iii) simultaneous measurement delay from both nodes '105' and '104.' As shown in Fig. 8(b.1), delays in different nodes manifest varying effects on convergence. Multiple-node communication delays may result in slower convergence or even divergence. All the phase voltages can be equally affected but not shown for brevity.

Concerning the replacement of unavailable measurements with pseudo-measurements of 1 *pu*, we conduct three experiments: (i) unavailability of measurements from node '105,' (ii) unavailability of measurements from node '104,' and (iii) unavailability of measurements from both nodes '105' and '104.' Comparative analysis between Figs. 8(b.1) and 8(c.1) suggest that the absence of measurements from multiple nodes appears to have a comparatively lesser impact. This could be because the unavailability of a measurement from a node implies the absence of a corresponding control objective in (1). This is also the reason the controllers reach a new operating point with a better control objective than that of with all measurements available, as shown in Fig. 8(c.1). Notably, in contemporary IP-based communication systems, measurements may include timestamps – which could be utilized before deploying the delayed signals with significant improvement in a performance gain.

C. Time-Varying Case for Synthetic Austin Grid

Here, we evaluate the performance of the *SZO-HLF-PGD* algorithm under time-varying load and generation conditions, as detailed in Section III in the presence of traditional voltage control devices. Parameters chosen are given as $\delta = 0.03$, ω, $\alpha = 0.6$, $k = 1 \times 10^{-7}$. OLTCs and SVRs are supplied with their respective setpoints, while ZO controllers operate independently based on measurements obtained from the example feeder illustrated in Fig. 4. The impact of ZO controllers providing set-points to conventional regulation devices is evident

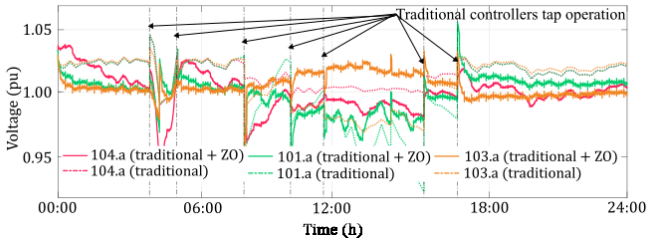

Fig. 9. Voltage profile with time-varying load profile in synthetic Austin grid feeder with OLTCs, SVRs, with diverse PVs, numerous controllers, and monitoring nodes to demonstrate *HLF-SZO-PGD* controller algorithm scalability. The voltages shown in this figure correspond to Phase A only.

in Fig. 9. Here, OLTCs and SVRs receive setpoint adjustments multiple times during the day (approximately at 08:00, 10:00, 12:00, 15:00, and 17:00 hours, denoted by vertical dotted lines). The operation of traditional voltage controllers introduces complexities due to varying tap set points assigned to different phases, subsequently affecting the performance of other phases. Notably, despite having no communication among the controllers, the ZO controllers are able to respond to exogenous sharp voltage change induced by the traditional controllers while limiting the voltages within reliability limits. It can also be seen (not shown for brevity) that while additional control actions significantly reduce reactive power demand from the ZO controllers, optimizing the setpoints provided to traditional controllers becomes imperative to minimize reactive power output from the ZO controllers while enhancing voltage regulation. Instead of simultaneous control of multiple tap positions, tap operations could be coordinated considering the presence of ZO voltage controller dynamics for an even better voltage profile.

V. Conclusion

Through extensive tests utilizing both the 3-phase unbalanced IEEE 13-node and synthetic Austin grid feeder, we have compared the performance of both *ZO-PGD* and *HLF-SZO-PGD* algorithms. Our findings clearly establish the superiority of the developed *HLF-SZO-PGD* algorithm, attributing its enhanced performance with the incorporation of filters, which significantly improves gradient tracking without affecting the final solution. The impact of the probing signal on the convergence speed has been demonstrated. The incorporation of filters also adds to the robustness of the controller, where, as demonstrated, the addition of noise has a limited impact on the convergence speed. Delayed measurement availability can negatively affect the convergence, compared to replacing missing available measurements with constant measurements. The controller also reasonably tracks the nominal voltage near 1 *pu* during dynamic loading conditions with demand spikes and with PV penetration in addition to the presence of other controllers within the system. Future work will further investigate the speeding up and scaling up of the proposed *HLF-SZO-PGD* algorithms.

References

[1] D. K. Molzahn, F. Dorfler, H. Sandberg, S. H. Low, S. Chakrabarti, R. Baldick, and J. Lavaei, "A Survey of Distributed Optimization and Control Algorithms for Electric Power Systems," *IEEE Transactions on Smart Grid*, vol. 8, no. 6, pp. 2941–2962, Nov. 2017.

[2] H. J. Liu, W. Shi, and H. Zhu, "Hybrid Voltage Control in Distribution Networks Under Limited Communication Rates," *IEEE Transactions on Smart Grid*, vol. 10, no. 3, pp. 2416–2427, May 2019.

[3] N. Patari, A. K. Srivastava, and N. Li, "Distributed Optimal Voltage Control Considering Latency and Asynchronous Communication for Three Phase Unbalanced Distribution Systems," *IEEE Transactions on Power Systems*, vol. 38, no. 2, pp. 1033–1043, Mar. 2023.

[4] G. Qu and N. Li, "Optimal Distributed Feedback Voltage Control Under Limited Reactive Power," *IEEE Transactions on Power Systems*, vol. 35, no. 1, pp. 315–331, Jan. 2020.

[5] P. S. Sarker, S. Majumder, M. F. Rafy, and A. K. Srivastava, "Impact Analysis of Cyber-Events on Distributed Voltage Control with Active Power Curtailment," in *2022 IEEE International Conference on Power Electronics, Drives and Energy Systems (PEDES)*. Jaipur, India: IEEE, Dec. 2022, pp. 1–6.

[6] S. Majumder, A. Vosughi, H. M. Mustafa, T. E. Warner, and A. K. Srivastava, "On the Cyber-Physical Needs of DER-Based Voltage Control/Optimization Algorithms in Active Distribution Network," *IEEE Access*, vol. 11, pp. 64 397–64 429, 2023.

[7] X. Chen, G. Qu, Y. Tang, S. Low, and N. Li, "Reinforcement Learning for Decision-Making and Control in Power Systems," in *Women in Power: Research and Development Advances in Electric Power Systems*, ser. Women in Engineering and Science. Cham: Springer International Publishing, 2023, pp. 265–285.

[8] X. Chen, J. I. Poveda, and N. Li, "Model-Free Optimal Voltage Control via Continuous-Time Zeroth-Order Methods," *arXiv preprint arXiv:2103.14703*, 2021.

[9] ——, "Model-free feedback constrained optimization via projected primal-dual zeroth-order dynamics," *arXiv preprint arXiv:2206.11123*, 2022.

[10] ——, "Continuous-time zeroth-order dynamics with projection maps: Model-free feedback optimization with safety guarantees," *arXiv preprint arXiv:2303.06858*, 2023.

[11] K. B. Ariyur and M. Krstic, *Real-Time Optimization by Extremum-Seeking Control*. John Wiley & Sons, 2003.

[12] J. I. Poveda and N. Li, "Robust hybrid zero-order optimization algorithms with acceleration via averaging in time," *Automatica*, vol. 123, p. 109361, 2021.

[13] D. B. Arnold, M. Negrete-Pincetic, M. D. Sankur, D. M. Auslander, and D. S. Callaway, "Model-Free Optimal Control of VAR Resources in Distribution Systems: An Extremum Seeking Approach," *IEEE Transactions on Power Systems*, vol. 31, no. 5, pp. 3583–3593, Sep. 2016.

[14] H. Nazaripouya, H. R. Pota, C.-C. Chu, and R. Gadh, "Real-Time Model-Free Coordination of Active and Reactive Powers of Distributed Energy Resources to Improve Voltage Regulation in Distribution Systems," *IEEE Transactions on Sustainable Energy*, vol. 11, no. 3, pp. 1483–1494, Jul. 2020.

[15] X. Li, Y. Li, J. E. Seem, and P. Lei, "Maximum power point tracking for photovoltaic systems using adaptive extremum seeking control," in *IEEE Conference on Decision and Control and European Control Conference*. Orlando, FL, USA: IEEE, Dec. 2011, pp. 1503–1508.

[16] J. Johnson, A. Summers, R. Darbali-Zamora, J. Hernandez-Alvidrez, J. Quiroz, D. Arnold, and J. Anandan, "Distribution Voltage Regulation Using Extremum Seeking Control With Power Hardware-in-the-Loop," *IEEE Journal of Photovoltaics*, vol. 8, no. 6, pp. 1824–1832, Nov. 2018.

[17] S. Liu, P.-Y. Chen, B. Kailkhura, G. Zhang, A. O. Hero III, and P. K. Varshney, "A primer on zeroth-order optimization in signal processing and machine learning: Principals, recent advances, and applications," *IEEE Signal Processing Magazine*, vol. 37, no. 5, pp. 43–54, 2020.

[18] X. Chen, Y. Tang, and N. Li, "Improve single-point zeroth-order optimization using high-pass and low-pass filters," in *International Conference on Machine Learning*. PMLR, 2022, pp. 3603–3620.

[19] R. C. Dugan and T. E. McDermott, "An open source platform for collaborating on smart grid research," in *2011 IEEE Power and Energy Society General Meeting*, Jul. 2011, pp. 1–7.

[20] V. Kekatos, L. Zhang, G. B. Giannakis, and R. Baldick, "Voltage Regulation Algorithms for Multiphase Power Distribution Grids," *IEEE Transactions on Power Systems*, vol. 31, no. 5, pp. 3913–3923, Sep. 2016.

[21] D. P. Bertsekas, *Nonlinear Programming*, 2nd ed. Belmont, Mass: Athena scientific, 1999.

[22] Y. Tan, D. Nešić, and I. Mareels, "On the choice of dither in extremum seeking systems: A case study," *Automatica*, vol. 44, no. 5, pp. 1446–1450, May 2008.

[23] W. Tao, S. Long, G. Wu, and Q. Tao, "The role of momentum parameters in the optimal convergence of adaptive polyak's heavy-ball methods," *arXiv preprint arXiv:2102.07314*, 2021.

[24] X. Yi, S. Zhang, T. Yang, T. Chai, and K. H. Johansson, "Linear convergence of first-and zeroth-order primal–dual algorithms for distributed nonconvex optimization," *IEEE Transactions on Automatic Control*, vol. 67, no. 8, pp. 4194–4201, 2021.

[25] A. B. Birchfield, T. Xu, K. M. Gegner, K. S. Shetye, and T. J. Overbye, "Grid Structural Characteristics as Validation Criteria for Synthetic Networks," *IEEE Transactions on Power Systems*, vol. 32, no. 4, pp. 3258–3265, Jul. 2017.

[26] "Pecan Street – Pecan Street Inc." [Online]. Available: https://www.pecanstreet.org/about/

[27] Y. Tan, W. H. Moase, C. Manzie, D. Nesic, and I. M. Y. Mareels, "Extremum seeking from 1922 to 2010," in *Proceedings of the 29th Chinese Control Conference*. Beijing, China: IEEE, 2010, pp. 14–26.